

Supporting Information

**Immobilizing tBP via Tailor-made π -Conjugated Hole Transport Materials
for Efficient and Stable Perovskite Solar Cells**

Daqing Zhang¹, Qianxin Long¹, Bihui Sun², Xin Luo², Guorong Zhou², Jinhai Huang³, Zhiyun Zhang^{1}, Jianhua Su¹, and Bo Xu^{2*}*

¹Key Laboratory for Advanced Materials and Institute of Fine Chemicals, School of Chemistry and Molecular Engineering, East China University of Science and Technology, Shanghai 200237, P. R. China

²School of Chemistry and Chemical Engineering, School of Materials Science and Engineering, Nanjing University of Science and Technology, Nanjing 210094, P. R. China

³Shanghai NanoShine Technology Co., Ltd, Shanghai 200030, P. R. China

* Email: boxu@njust.edu.cn (Bo Xu); zhangzhiyun@ecust.edu.cn (Zhiyun Zhang)

Characterization

Characterization

All the reagents and solvents were directly purchased from commercial companies (Shanghai Haohong Scientific Co., Ltd) without further purification. The ^1H and ^{13}C nuclear magnetic resonance (NMR) spectra were characterized from a Bruker AM600 spectrometer. The mass spectrometry (MS) was measured by a waters LCT premier XE spectrometer. The ultraviolet-visible (UV-Vis) absorption spectra were recorded in solutions on an Agilent spectrophotometer while PL delay spectra were measured on Edinburgh Instruments Fluorescence Spectrometer (FLS1000). Thermogravimetric analysis (TGA) was carried out using a SHIMADZU TGA-50/50H instrument under a nitrogen atmosphere with a heating scan rate of $10\text{ }^\circ\text{C}\cdot\text{min}^{-1}$ from 30 to 600 $^\circ\text{C}$. The differential scanning calorimetry (DSC) analysis was confirmed from a SHIMADZU DSC-60Plus instrument under nitrogen atmosphere with a heating scan rate of $20\text{ }^\circ\text{C}\cdot\text{min}^{-1}$ from 30 to 300 $^\circ\text{C}$. Atomic force microscopy (AFM) measurements were recorded by using a Dimension 3100 Scanning Probe Microscope at ambient temperature in tapping mode. The contact angles were tested by using a contact angle meter model SL150 (USA KINO Industry). Scanning electron microscope (SEM) images were undertaken with a TESCAN VEGA 3 SBH.

Electrochemical Measurements

Electrochemical experiments were performed with a CH Instruments electrochemical workstation (model 660A) using a conventional three-electrode electrochemical cell. A tetrahydrofuran solution (THF) containing 0.1 M of tetrabutylammoniumhexafluorophosphate ($n\text{-Bu}_4\text{NPF}_6$) was introduced as the electrolyte, where an $\text{Ag}/0.01\text{ M AgNO}_3$ electrode (acetonitrile as solvent) was used as the reference electrode and a glassy carbon disk (diameter

3 mm) as the working electrode, a platinum wire as the counter electrode. The cyclic voltammetry scan rates were 50 mV/s. All redox potentials were calibrated vs. normal hydrogen electrode (NHE) by the addition of the ferrocene potential. The conversion $E_{(Fc/Fc^+)} = 630 \text{ mV vs NHE}$.

HOMO and LUMO energy level calculation

The calculation formulas for optical bandgap (E_g), HOMO energy level, and LUMO energy level are as follows:

$$E_g = \frac{1241}{\lambda_{onset}}$$

$$E_{HOMO} = -\left(E_1^{OX} + 4.4\right) \frac{1}{2}$$

$$E_{LUMO} = E_{HOMO} + E_g$$

Where λ_{onset} is the wavelength corresponding to the onset of the normalized absorption

spectrum, $\frac{E_1^{OX}}{2}$ is the half-wave potential of the reversible process. E_{HOMO} was standardized with ferrocene.

Computational Details

In the simulation, optimization and single point energy calculations are performed using the cam-B3LYP and the 6-31G* basis set for all atoms, without any symmetrical constraints. All reported calculations were carried out by means of Gaussian 09.^[1] The reorganization energy λ , is determined by four energies, (the Nelson four-point method):

$$\lambda = E_+^* - E_+ + E^* - E$$

Where the E_+^* is the energy of the neutral molecule in the cation symmetry, and the E^* is the energy of the cationic molecule in the neutral symmetry; the E_+ and E are the optimized energies of the cationic and neutral molecules.

Mobility Measurements

Hole mobility was investigated by the space-charge-limited current (SCLC) method, which can be described by the following equation:

$$J = \frac{9}{8} \mu \epsilon_0 \epsilon_r \frac{V^2}{d^3}$$

Where J is the current density, μ is the hole mobility, ϵ_0 is the vacuum permittivity (8.85×10^{-12} F/ m), ϵ_r is the dielectric constant of the material (normally taken to approach 3 for organic semiconductors), V is the applied bias, and d is the film thickness. The hole-only devices were fabricated according to the literature procedures.^[2]

Conductivity Measurements

The formula for calculating conductivity is as follows:

$$\sigma = \frac{IL}{VA}$$

Where L is the thickness of HTM, I is the dark current, V is the applied voltage, and A is the effective area of the device.

The conductivities of the HTMs were determined by using a two-contact electrical conductivity set-up, which was performed by following published procedures.^[3] Glass substrates without the conductive layer were carefully cleaned in ultrasonic baths of detergents, deionized water, acetone, and ethanol successively. The remaining organic residues were removed within 10 min by airbrushing. A thin layer of nanoporous TiO_2 was coated on the glass substrates by spin-

coating with a diluted TiO₂ paste (Dyesol DSL 18NR-T) with terpineol (1:3, mass ratio). The thickness of the film is ca. 500 nm, as measured with a DekTak profilometer. After sintering the TiO₂ film on a hotplate at 500 °C for 30 min, the film was cooled to room temperature, before it was subsequently deposited by spin-coating a solution of HTM in chlorobenzene, whereas the concentrations and additives were the same as in the case of photovoltaic devices. Subsequently, a 200 nm thick Ag back contact was deposited onto the organic semiconductor by thermal evaporation in a vacuum chamber with a base pressure of about 10⁻⁶ bar, to complete the device fabrication. *J-V* characteristics were recorded on a Keithley 2400 Semiconductor Characterization System.^{[3][4]}

Steady-state PL and TRPL

The PL was measured by using FTO/TiO₂/Perovskite with and without HTM layer. An excitation wavelength of 460 nm was used. The time-resolved photoluminescence (TRPL) curve fitting adopts a two-component formula, and the specific TRPL and average PL lifetime (τ_{avg}) formula is as follows:

$$y = A_1 \exp\left(\frac{-t}{\tau_1}\right) + A_2 \exp\left(\frac{-t}{\tau_2}\right) + A_0$$

$$\tau_{avg} = \frac{A_1 \tau_1^2 + A_2 \tau_2^2}{A_1 \tau_1 + A_2 \tau_2}$$

Where τ_1 is the fast decay process associated with the charge extraction, and τ_2 is the slow decay process related to the interface charge recombination, A_1 and A_2 are decay amplitudes^[5].

Hysteresis Index Calculation

The formula for calculating hysteresis index (HI) is as follows:

$$HI = \frac{PCE_{Reverse} - PCE_{Forward}}{PCE_{Reverse}} \times 100\%$$

Device Fabrication

N-i-p planar perovskite solar cells: FTO glass was cleaned by sequentially washing with detergent, deionized water, acetone, and ethyl alcohol and then dried under a nitrogen atmosphere. The substrates were treated with oxygen plasma for 15 min. The SnO₂ film was spin-coated using a commercial SnO₂ colloidal solution (diluted with DI water to adjust to 4 wt%) at 3000 rpm for 30 s, followed by annealing at 180 °C on a hot plate for 30 min. The perovskite film was deposited by spin coating onto the SnO₂ substrate. The perovskite layer was deposited by spin coating the perovskite precursor solution in one step, which was prepared by mixing of the formamidinium iodide (FAI), lead iodide (PbI₂), methylammonium bromide (MABr) and lead bromide (PbBr₂) in a mixed solvent of DMF and DMSO solution (volume ratio 4:1) with the molar concentration of 1.35M Pb²⁺ (PbI₂ and PbBr₂). The molar ratio of PbI₂/PbBr₂=85/15, PbI₂/FAI=1.05, PbBr₂/MABr=1/1. The spin coating procedure was done in an Argon flowing glovebox, first 2000 rpm for 10 s with a ramp of 200 rpm·s⁻¹, second 4000 rpm for 30 s with a ramp of 2000 rpm·s⁻¹. 200 μl chlorobenzene was dropped on the spinning substrate during the second spin-coating step 20 s before the end of the procedure. The substrate was then heated at 100°C for 90 min on a hotplate. After cooling down to room temperature, HTM was subsequently deposited on the top of the perovskite layer by spin coating at 4000 rpm for 20 s. The HTM solutions were prepared by dissolving the HTM in chlorobenzene at a concentration of 70 mM, with the addition of 30 mM LiTFSI (from a stock solution in acetonitrile with concentration of 1.0 M), 200 mM of t-BP (from a stock solution in chlorobenzene with concentration of 1.0 M) and 1.8 mM FK209 (from a stock solution in acetonitrile with concentration of 0.5 M). The HTM solution was dripped on the perovskite electrode and then followed by spin-coating for 30 s at 3000 rpm. All of the HTM solutions

were prepared in the glove box under a nitrogen atmosphere; chlorobenzene and acetonitrile were deaerated by bubbling with dry nitrogen for half hour before introducing into the glove box environment. Finally, 80 nm of gold was deposited by thermal evaporation using a shadow mask to pattern the electrodes.^[6]

P-i-n inverted perovskite solar cells: The indium tin oxide (ITO) coated glass substrates were sequentially cleaned with a detergent, deionized water, acetone, and ethanol. Afterward, the substrates were placed in a drying oven and dried at 80 °C for 30 minutes. Subsequently, the dried substrates underwent UV-ozone plasma treatment for 15 min. After cooling down to room temperature, HTM was subsequently deposited on the top of the ITO by spin coating at 4000 rpm for 20 s. The HTM solutions were prepared by dissolving the HTM in chlorobenzene at a concentration of 10 mg/mL. Subsequently, the perovskite solution of $\text{FA}_{0.76}\text{MA}_{0.20}\text{Cs}_{0.04}\text{Pb}(\text{I}_{0.96}\text{Cl}_{0.04})_3$ was prepared by adding 824 mg of PbI_2 , 237.5 mg of FAI, 21.1 mg of CsI, 13.6 mg of MACl and 25.83 mg of MAI into mixed solvent of 800 μL DMF and 200 μL DMSO. The perovskite solution was spin-coated at 1000 rpm for 10 s and then at 4000 rpm for 30 s. In the last 15 s of the second step, the 150 μL CB was dropped into the center of the sample quickly. Then, it was annealed on a hot plate at 100 °C for 30 min. Finally, the substrates were transferred to a vacuum chamber to evaporate 25 nm C60, 5 nm BCP, and 100 nm Ag, sequentially.^[7]

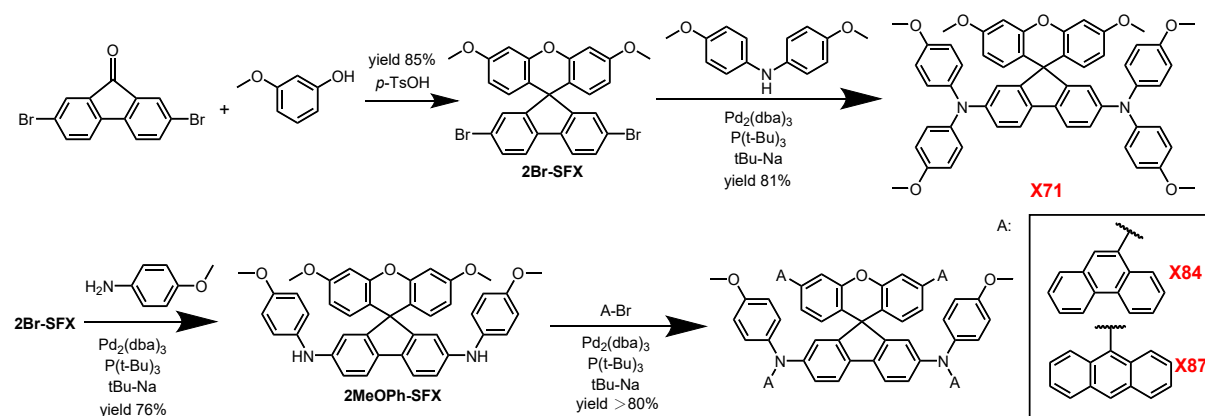
Device Characterization

Current-Voltage characteristics were recorded by applying an external potential bias to the cell while recording the generated photocurrent with a Keithley model 2400 digital source meter. The light source was a 300 W collimated xenon lamp (Newport) calibrated with the light intensity of 100 $\text{mW}\cdot\text{cm}^{-2}$ at AM 1.5 G solar light condition by a certified silicon solar cell (Fraunhofer ISE). IPCE spectra were recorded on a computer-controlled setup comprised of a

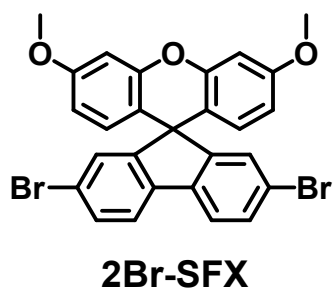
xenon lamp (Spectral Products ASB-XE-175), a monochromator (Spectral Products CM110), and a Keithley multimeter (Model 2700). The setup was calibrated with a certified silicon solar cell (Fraunhofer ISE) prior to measurements. The prepared PSC samples were masked during the measurement with an aperture area of 0.126 cm² (diameter 4 mm) exposed under illumination. The prepared PSC samples were masked during the measurement with an aperture area of 0.2 cm² exposed under illumination.

Experimental Section

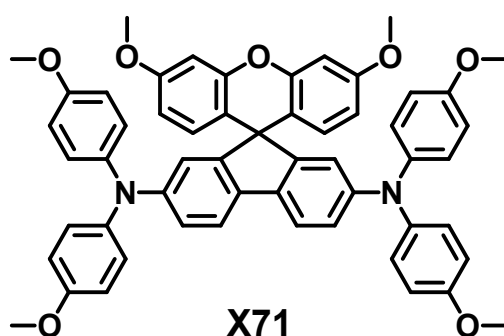
Chemicals: 2,7-dibromo-9-fluorenone, 3-Methoxyphenol, 9-Bromoanthracene, 9-Bromophenanthrene, *p*-toluenesulfonic acid, 4-methoxyaniline, Sodium tert-butoxide, Tri-tert-butylphosphine, Palladium(II) acetate, Chlorobenzene (anhydrous 99.8%), acetonitrile (anhydrous 99.8%) were purchased from commercial companies (Shanghai Haohong Scientific Co., Ltd) without further purification. Solvents and other chemicals are commercially available and used as received unless specially stated. Chromatography was performed using silica gel 60Å (35-63 μm).



Scheme S1. Synthetic routes for **X71**, **X84** and **X87**.

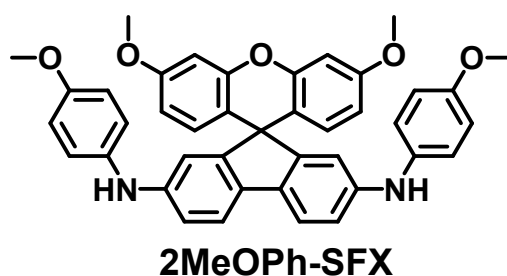


Synthesis of 2,7-dibromo-3',6'-dimethoxyspiro[fluorene-9,9'-xanthene] (2Br-SFX): 2,7-dibromo-9-fluorenone (1.0 g, 3.0 mmol), 3-methoxyphenol (1.5 g, 12.0 mmol), *p*-TsOH (60 mg, 0.3 mmol), and toluene (15 mL) were added to a two-necked flask. The mixture was refluxed for 10 h, and then cooled to room temperature. After methanol (150 mL) was added, the mixture was stirred for 0.5 h. The white precipitated from the reaction mixture was isolated by filtration. The crude product was washed by methanol (50 mL) and filtrated to obtain the product **2Br-SFX** as the white powder (1.4 g, yield 85%). ¹H NMR (500 MHz, *d*₆-DMSO, 298 K), δ (ppm): 7.97 (d, *J* = 10 Hz, 2H), 7.61 (dd, *J* = 10 Hz, 2H), 7.15 (s, 2H), 6.83 (s, 2H), 6.48 (dd, *J* = 10 Hz, 2H), 6.18 (d, *J* = 15 Hz, 2H), 3.74 (s, 6H, OMe). ¹³C NMR (125 MHz, *d*₆-DMSO, 298 K), δ (ppm): 159.47, 156.84, 151.22, 137.31, 131.26, 128.25, 127.84, 122.88, 121.64, 114.35, 111.03, 101.39, 55.33, 52.83.



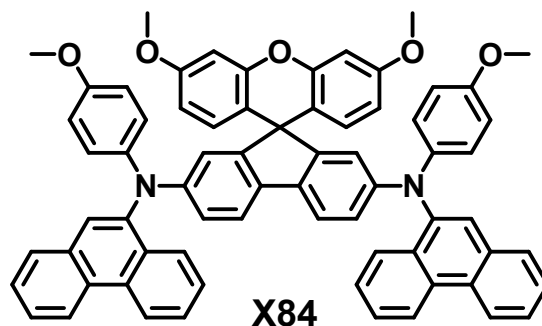
Synthesis of 3',6'-dimethoxy-N²,N²,N⁷,N⁷-tetrakis(4-methoxyphenyl)spiro[fluorene-9,9'-xanthene]-2,7-diamine (X71): 2,7-dibromo-3',6'-dimethoxyspiro[fluorene-9,9'-xanthene] (2Br-SFX) (1.00 g, 1.81 mmol), bis(4-methoxyphenyl)amine (1.24 g, 5.45 mmol), Pd₂(dba)₃ (0.16 g, 0.18 mmol), P(*t*-Bu)₃ (0.07 g, 0.36 mmol) and sodium *t*-butoxide (0.52 g, 5.45 mmol)

were added into a three-necked flask and poured 10 mL of toluene, then heated up to 120 °C under nitrogen protection. After stirring for 8h, the reaction mixture was cooled to room temperature, washed with water, and being dried over magnesium sulphate. The product was purified by column chromatography to attain faint yellow solid (1.25 g, 81.16 %). ¹H NMR (500 MHz, *d*₆-DMSO, 298 K), δ (ppm): 7.56 (d, *J* = 10 Hz, 2H), 6.85 (d, *J* = 10 Hz, 8H), 6.78 (d, *J* = 10 Hz, 8H), 6.71 (d, *J* = 10 Hz, 2H), 6.67 (s, 2H), 6.55 (d, *J* = 10 Hz, 2H), 6.48 (s, 2H), 6.35 (d, *J* = 10 Hz, 2H), 3.74 (s, 6H, OMe), 3.69 (s, 12H, OMe). ¹³C NMR (125 MHz, *d*₆-DMSO, 298 K), δ (ppm): 159.03, 155.37, 155.21, 151.23, 147.50, 140.09, 131.78, 127.95, 125.98, 123.57, 119.97, 119.74, 116.84, 116.36, 114.70, 110.78, 100.87, 55.29, 55.13, 52.68. HR-MS (ESI) *m/z*: [M]⁺ calcd for 846.3305; found, 846.3280.

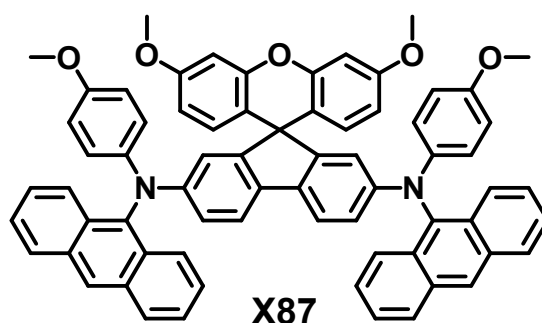


Synthesis of 3',6'-dimethoxy-*N*²,*N*⁷-bis(4-methoxyphenyl)spiro[fluorene-9,9'-xanthene]-2,7-diamine(2MeOPh-SFX): 2,7-dibromo-3',6'-dimethoxyspiro[fluorene-9,9'-xanthene] (5.00 g, 9.01 mmol), 4-methoxyaniline (4.47 g, 36.04 mmol), Pd₂(dba)₃ (0.16 g, 0.18 mmol), [(*t*-Bu)₃PH]BF₄ (0.10 g, 0.36 mmol) and sodium *t*-butoxide (2.59 g, 27.03 mmol) were added into a three-necked flask and poured 40 mL of toluene, then heated up to 120 °C under nitrogen protection. After stirring for 8h, the reaction mixture was cooled to room temperature, washed with water, and being dried over magnesium sulphate. The product was purified by column chromatography to attain the white solid (4.43 g, yield 76.85 %). ¹H NMR (600 MHz, *d*₆-DMSO, 298 K) δ 7.81 (s, 2H), 7.52 (d, *J* = 8.3 Hz, 2H), 6.91 (dd, *J* = 8.7, 2.4 Hz, 6H), 6.83 - 6.75 (m, 6H), 6.52 (dd, *J* = 8.8, 2.7 Hz, 2H), 6.50 (d, *J* = 2.1 Hz, 2H), 6.32 (d, *J* = 8.7 Hz, 2H),

3.75 (s, 6H), 3.68 (s, 6H). ^{13}C NMR (150 MHz, d_6 -DMSO, 298 K) δ 158.43, 155.32, 153.10, 150.56, 143.51, 135.34, 129.82, 128.12, 119.54, 118.93, 116.70, 113.89, 112.80, 111.34, 110.15, 100.32, 54.73, 54.57, 51.78.



Synthesis of 3',6'-dimethoxy- N^2,N^7 -bis(4-methoxyphenyl)- N^2,N^7 -di(phenanthren-9-yl)spiro[fluorene-9,9'-xanthene]-2,7-diamine (X84): The synthesis procedure of **X84** was the same as **X71** to give **X84** as light yellow solid (529 mg, yield 85 %). ^1H NMR (500 MHz, d_6 -DMSO, 298 K), δ (ppm): 8.82 (d, $J = 10$ Hz, 2H), 8.77 (d, $J = 10$ Hz, 2H), 7.77 (t, $J = 10$ Hz, 4H), 7.65~7.54 (m, 8H), 7.50 (s, 2H), 7.42 (t, $J = 10$ Hz, 2H), 6.96 (d, $J = 10$ Hz, 4H), 6.78 (d, $J = 10$ Hz, 4H), 6.73 (d, $J = 10$ Hz, 2H), 6.47 (d, $J = 10$ Hz, 2H), 6.43 (s, 4H), 6.30 (d, $J = 10$ Hz, 2H), 3.68 (s, 12H, OMe). ^{13}C NMR (125 MHz, d_6 -DMSO, 298 K), δ (ppm): 158.90, 155.33, 154.86, 151.14, 148.04, 141.58, 140.20, 131.75, 131.45, 129.07, 128.48, 127.97, 127.58, 126.98, 126.91, 126.80, 126.57, 125.79, 125.09, 124.37, 123.39, 122.74, 120.14, 119.03, 116.77, 115.80, 114.71, 110.57, 100.76, 55.18, 55.10, 52.72, 48.57. HR-MS (ESI) m/z : $[\text{M}]^+$ calcd for 986.3720; found, 986.3695.



Synthesis of N²,N⁷-di(anthracen-9-yl)-3',6'-dimethoxy-N²,N⁷-bis(4-methoxyphenyl)spiro [fluorene-9,9'-xanthene]-2,7-diamine (X87): The synthesis procedure of X87 was the same as X71 to give X87 as yellow solid (732 mg, yield 82 %). ¹H NMR (500 MHz, *d*₆-DMSO, 298 K), δ (ppm): 8.62 (s, 2H), 8.11 (d, J = 10 Hz, 4H), 7.83 (d, J = 10 Hz, 4H), 7.48~7.34 (m, 10H), 6.84 (d, J = 10 Hz, 4H), 6.69 (d, J = 10 Hz, 4H), 6.54 (d, J = 15 Hz, 6H), 6.43 (d, J = 15 Hz, 2H), 6.24 (d, J = 10 Hz, 2H), 3.73 (s, 6H, OMe), 3.62 (s, 6H, OMe). ¹³C NMR (125 MHz, *d*₆-DMSO, 298 K), δ (ppm): 158.93, 154.72, 154.50, 151.31, 147.82, 139.63, 136.59, 132.19, 131.25, 129.37, 128.95, 127.37, 126.77, 126.71, 125.46, 123.43, 122.89, 120.21, 117.32, 117.10, 114.58, 114.00, 110.50, 100.82, 55.24, 55.06. HR-MS (ESI) m/z: [M]⁺ calcd for 986.3720; found, 986.3725.

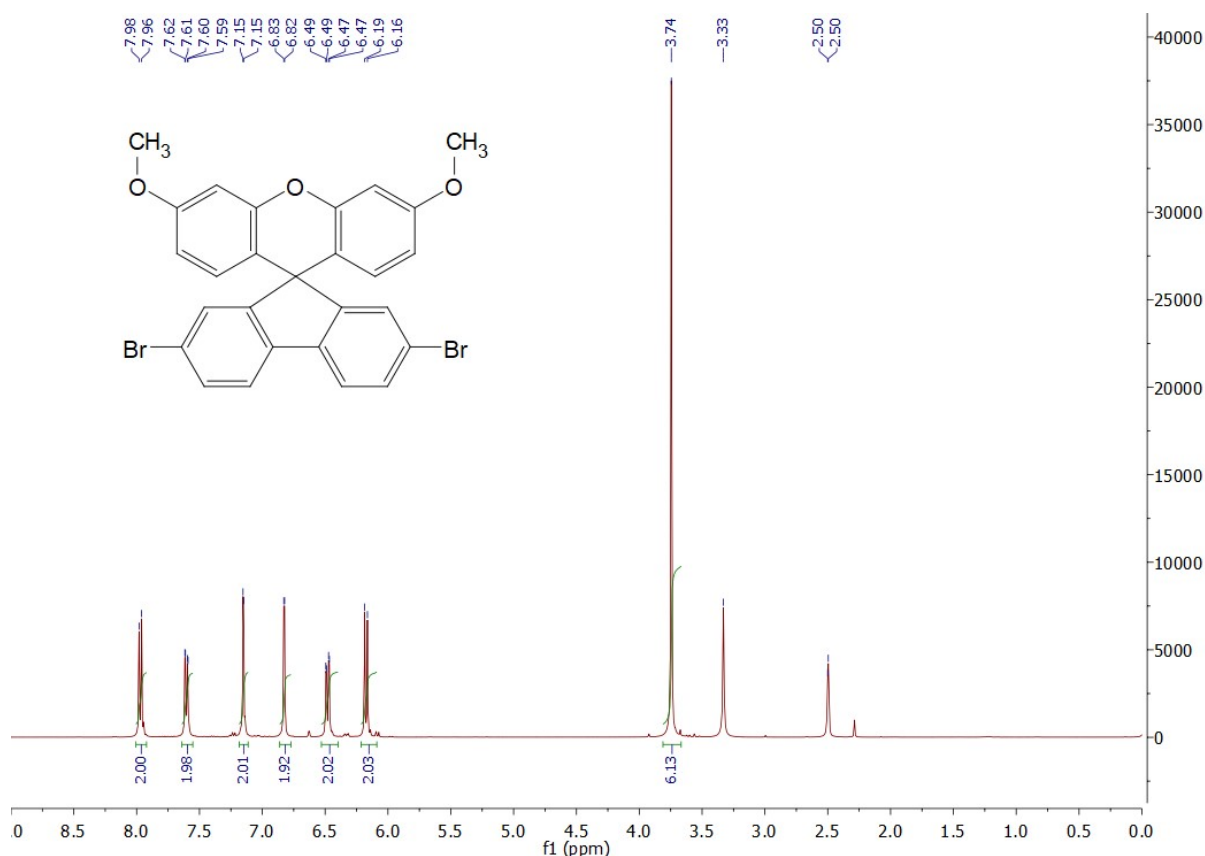


Figure S1. ¹H NMR (*d*₆-DMSO) spectrum of 2Br-SFX.

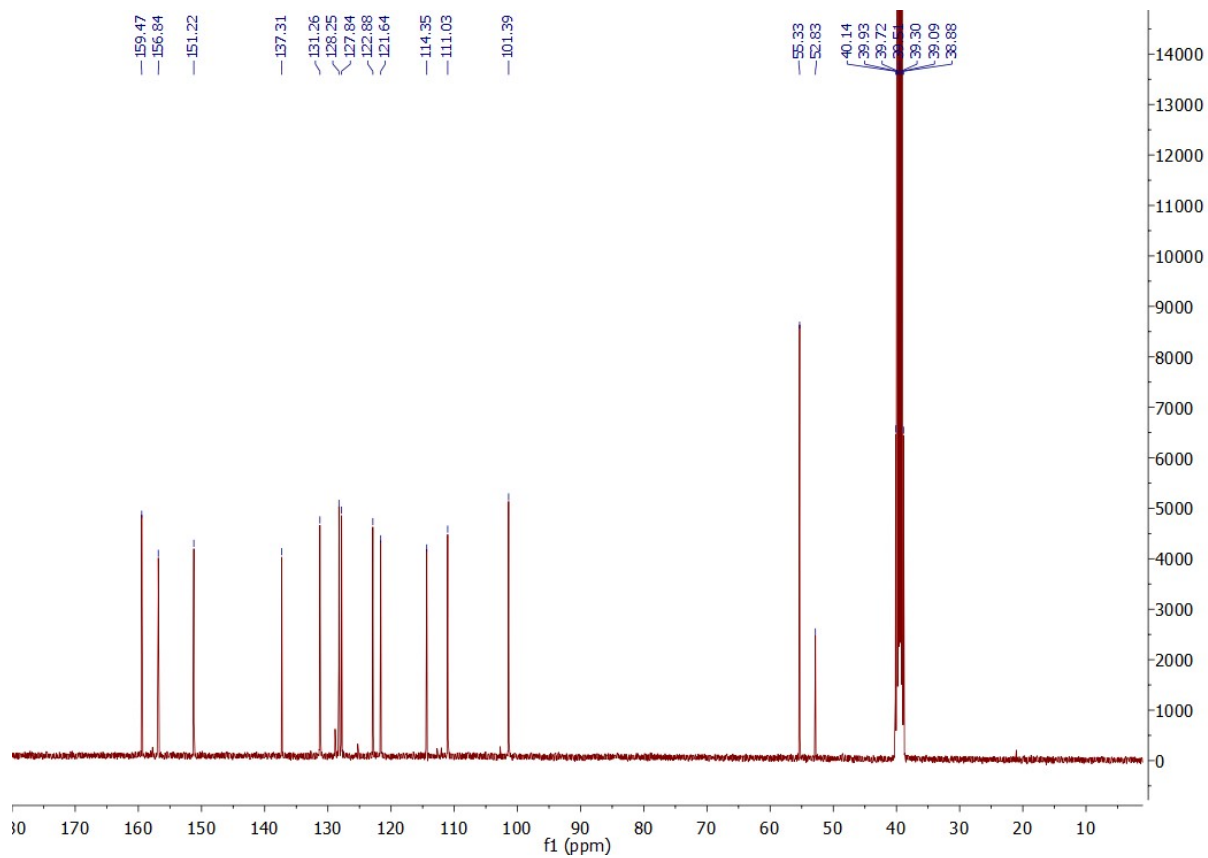


Figure S2. ¹³C NMR (*d*₆-DMSO) spectrum of **2Br-SFX**.

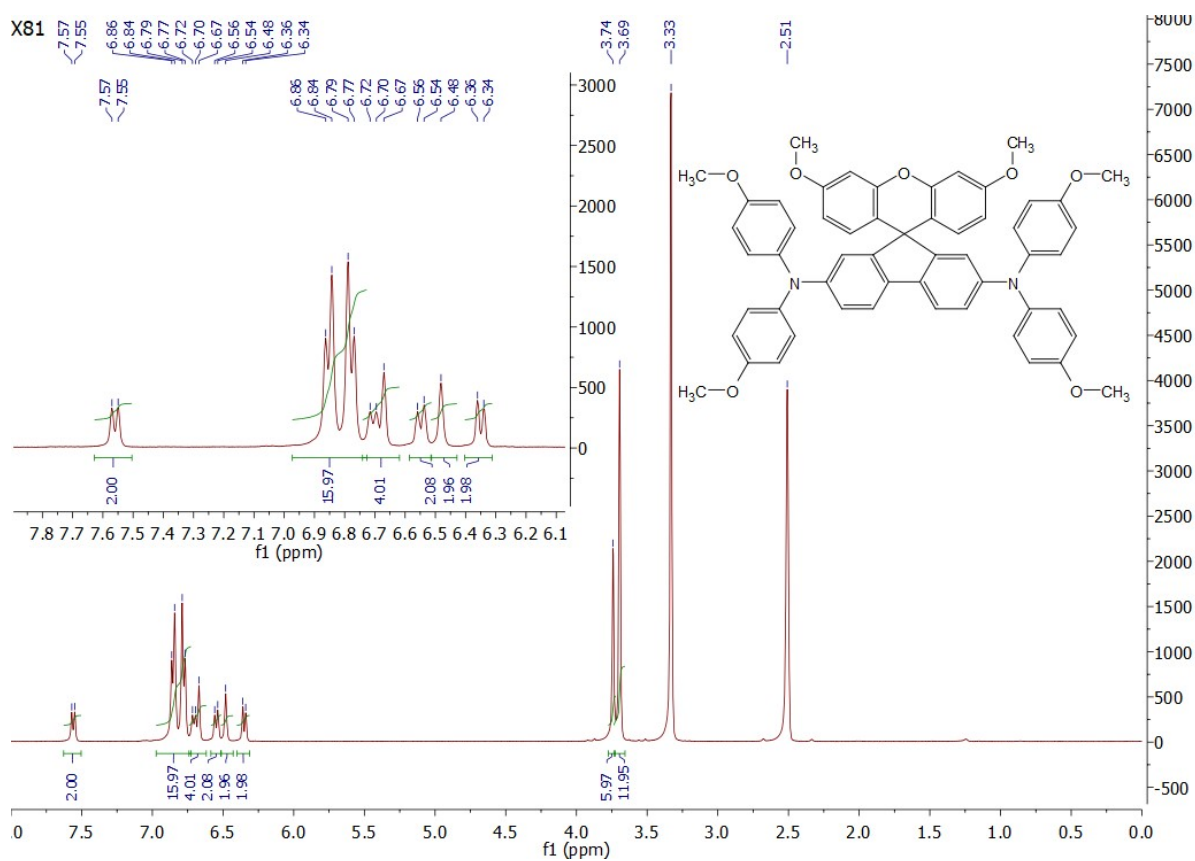


Figure S3. ^1H NMR (d_6 -DMSO) spectrum of X71.

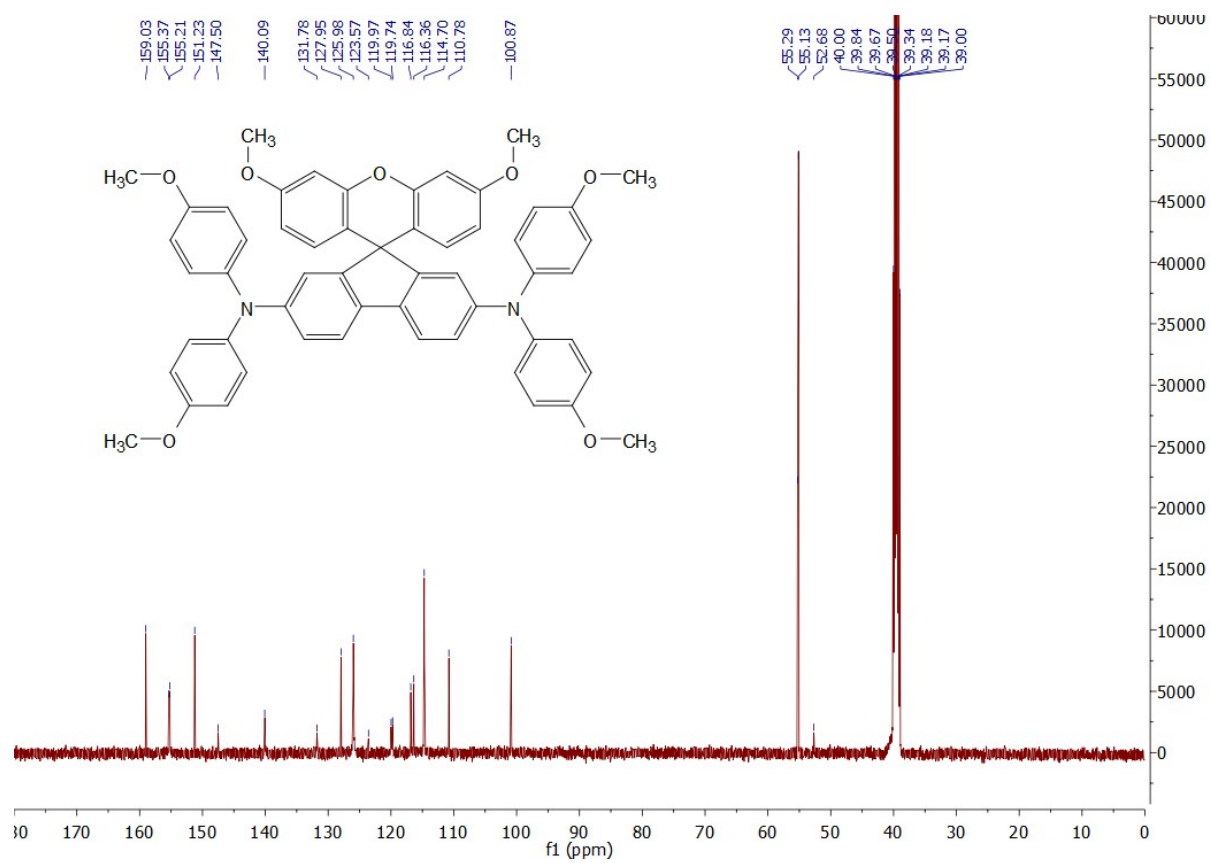


Figure S4. ^{13}C NMR (d_6 -DMSO) spectrum of X71.

SmartFormula

Formula	Mass	Error	mSigma	DblEq	N rule	Electron Configuration
$C_{55}H_{46}N_2O_7$	846.3305	3.0108	13.8908	34.00	ok	odd

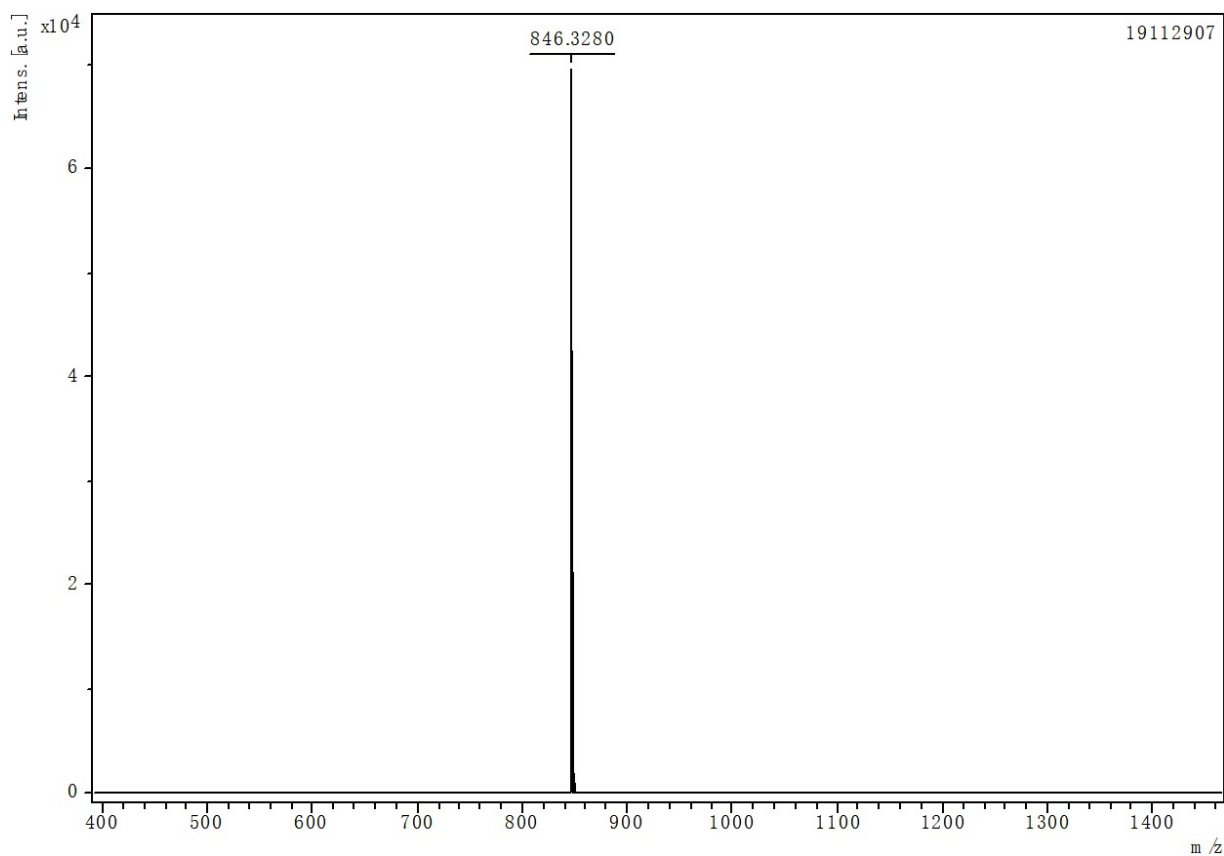


Figure S5. HR-MS spectra of **X71**.

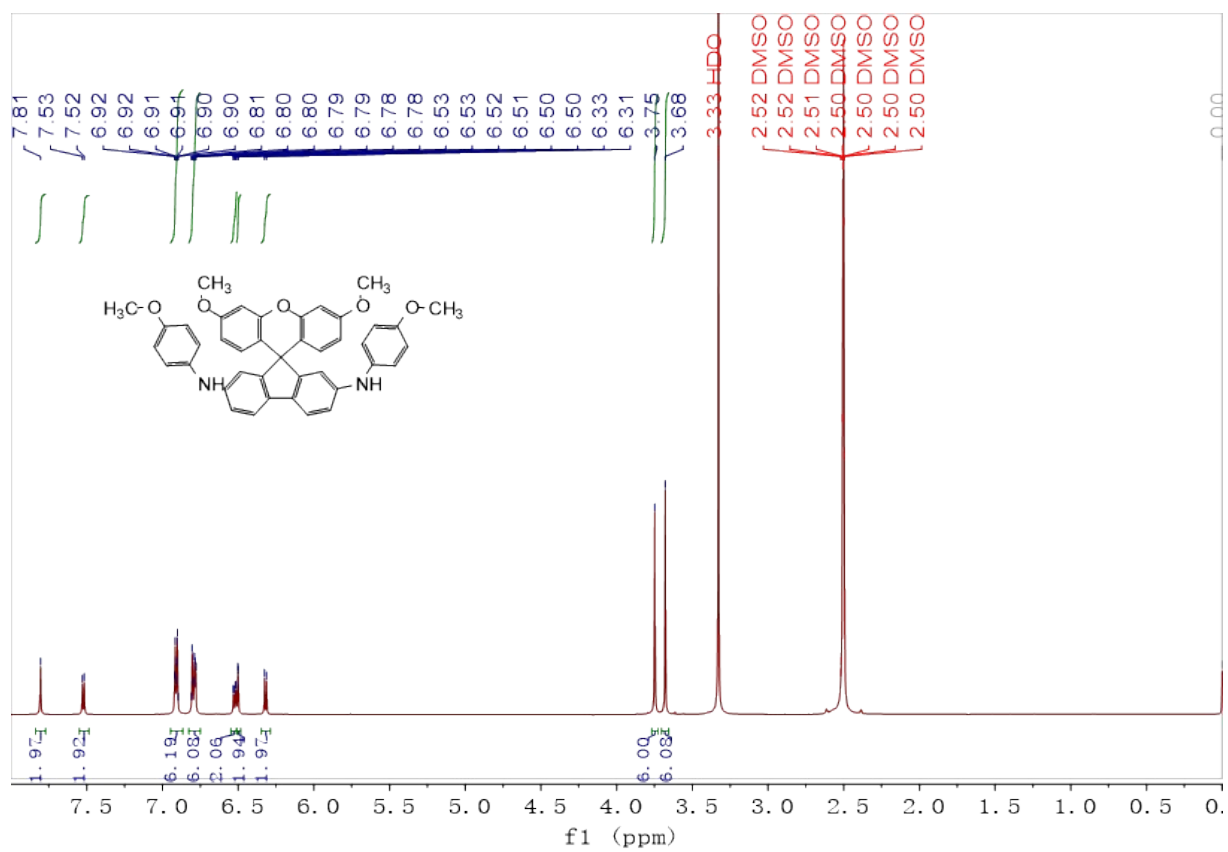


Figure S6. ^1H NMR (d_6 -DMSO) spectrum of 2MeOPh-SFX.

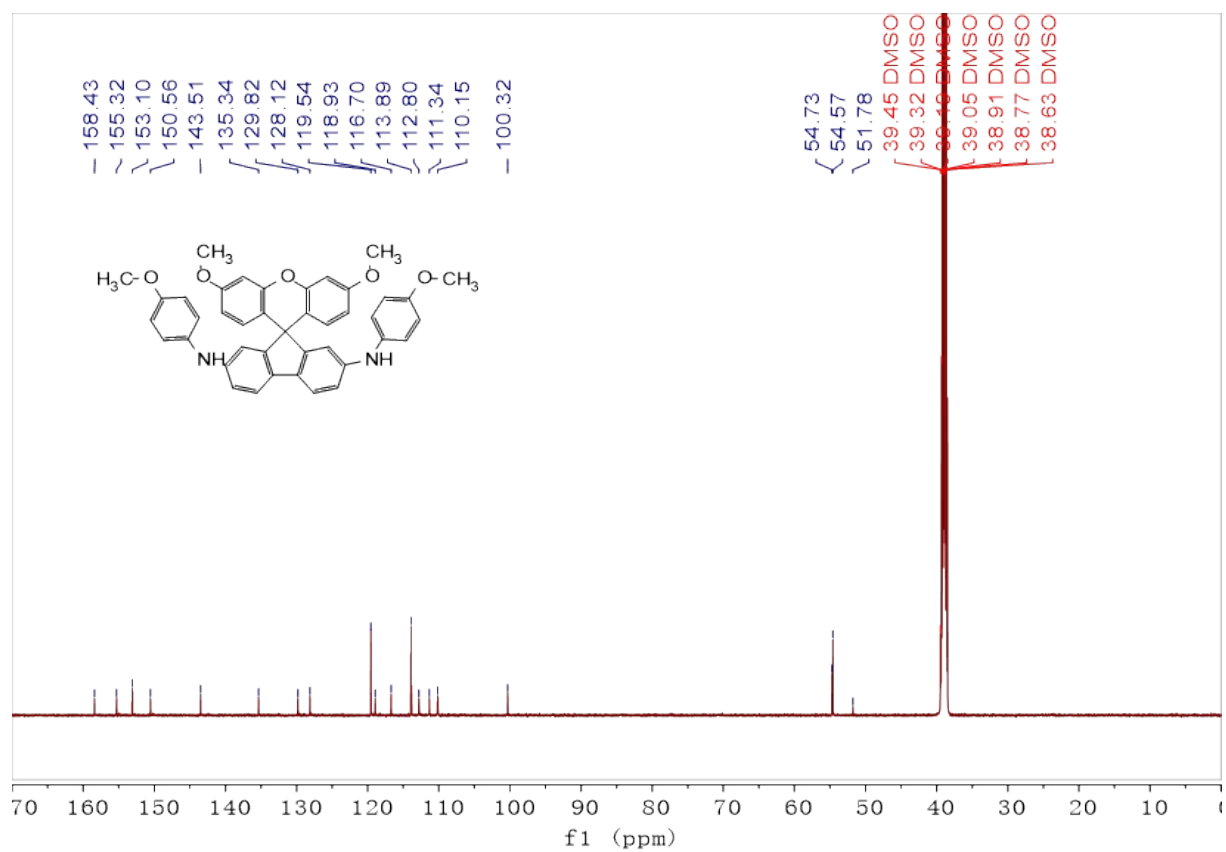


Figure S7. ¹³C NMR (d₆-DMSO) spectrum of 2MeOPh-SFX.

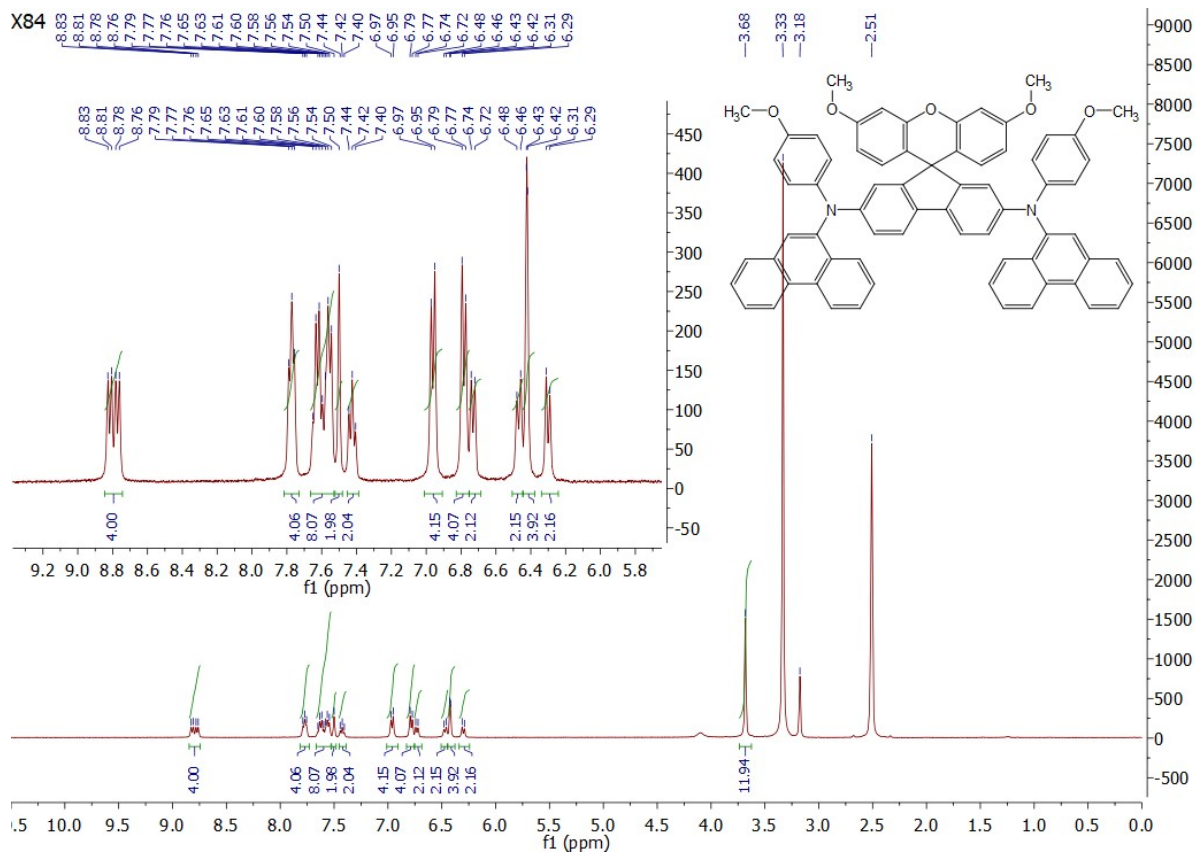


Figure S8. ^1H NMR (d_6 -DMSO) spectrum of X84.

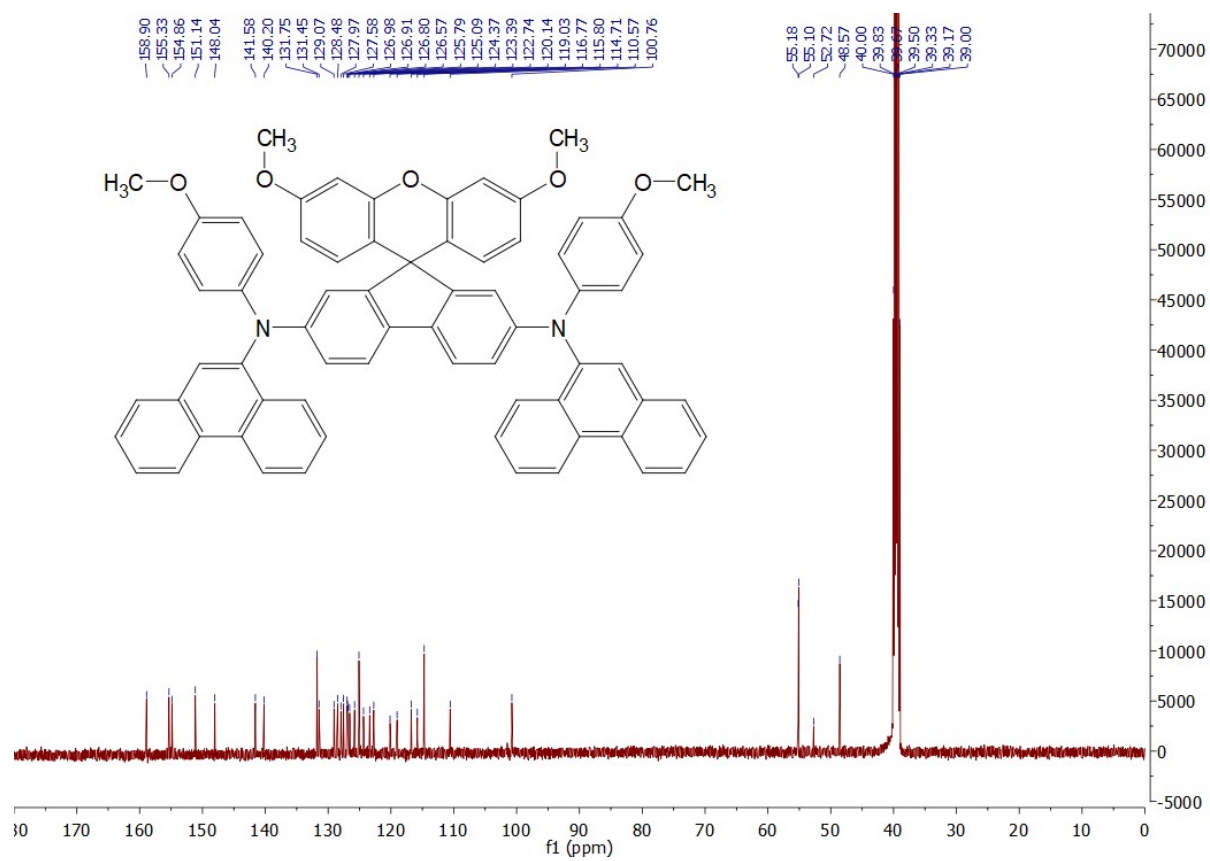


Figure S9. ^{13}C NMR (d_6 -DMSO) spectrum of X84.

SmartFormula

Formula	Mass	Error	mSigma	DbIEq	N rule	Electron Configuration
C ₆₉ H ₅₀ N ₂ O ₅	986.3720	2.4609	45.4113	46.00	ok	odd

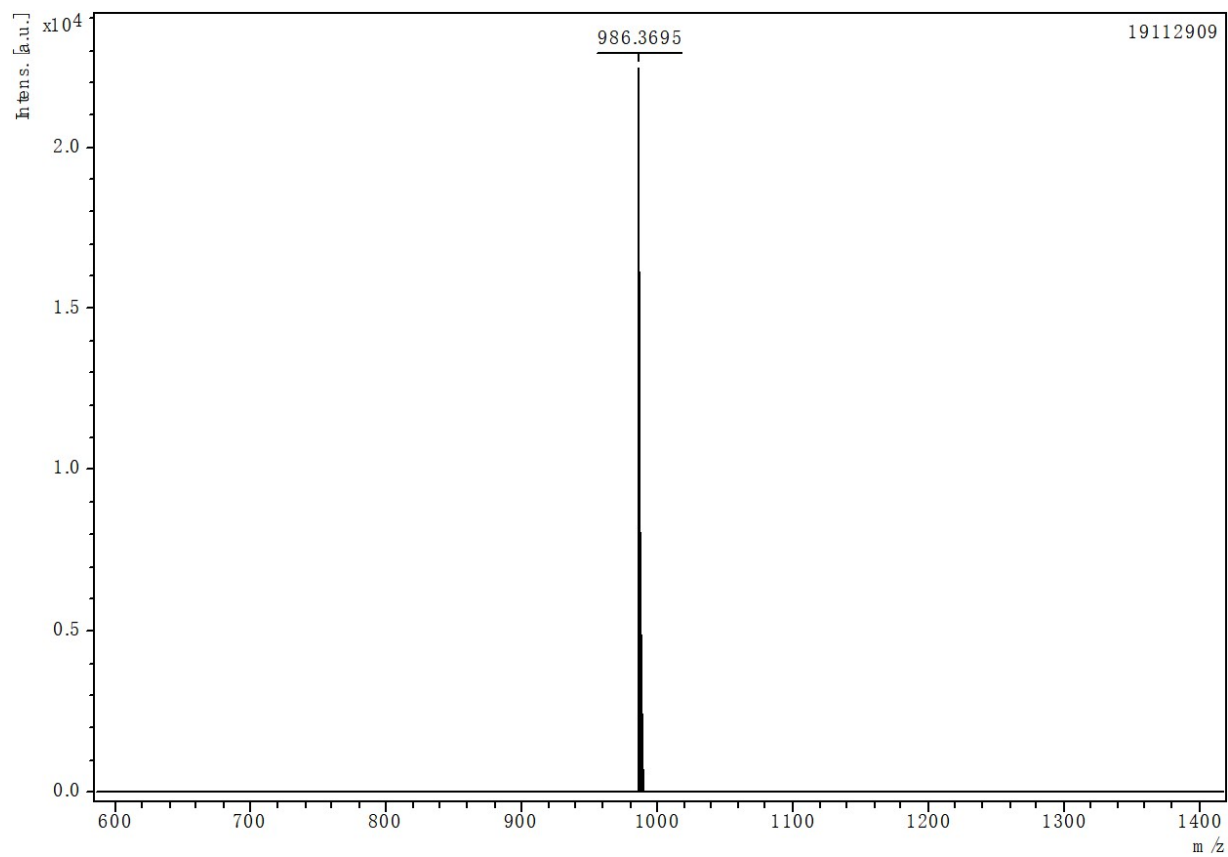


Figure S10. HR-MS spectra of **X84**.

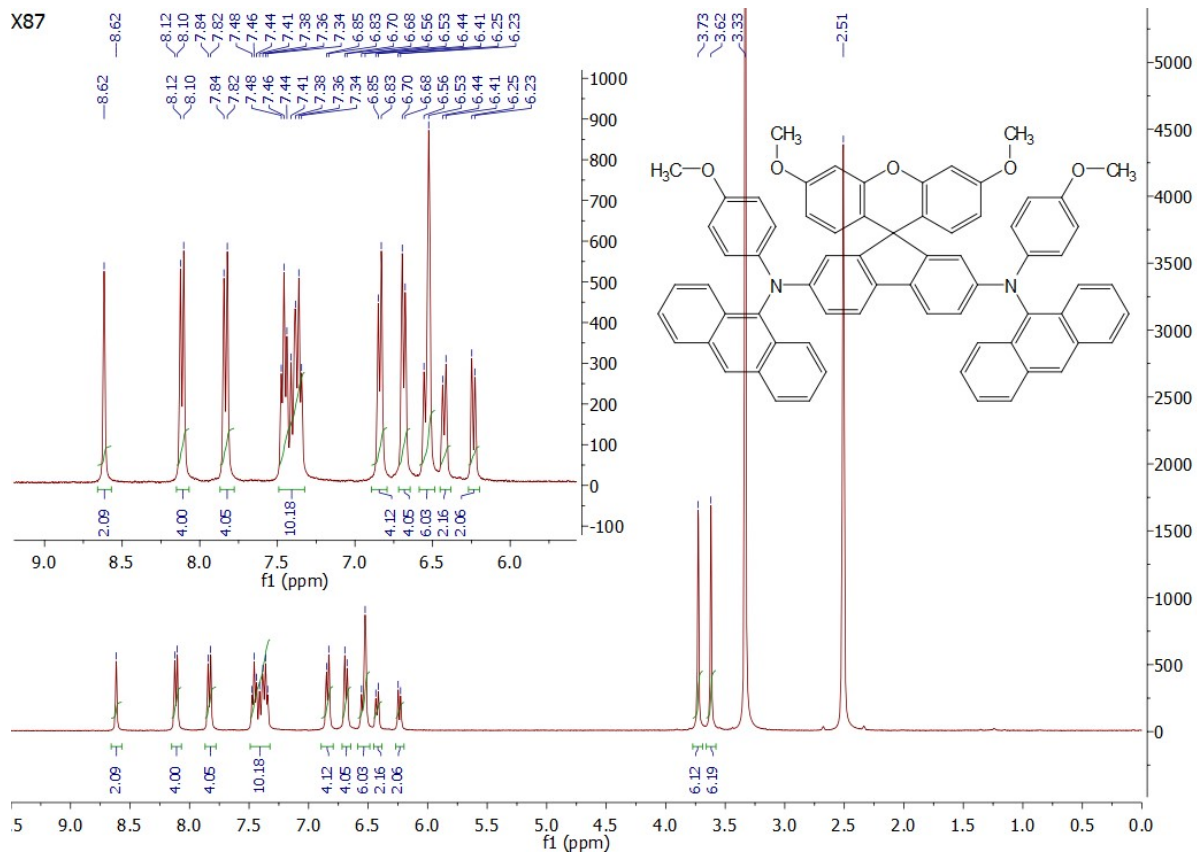


Figure S11. ^1H NMR (d_6 -DMSO) spectrum of X87.

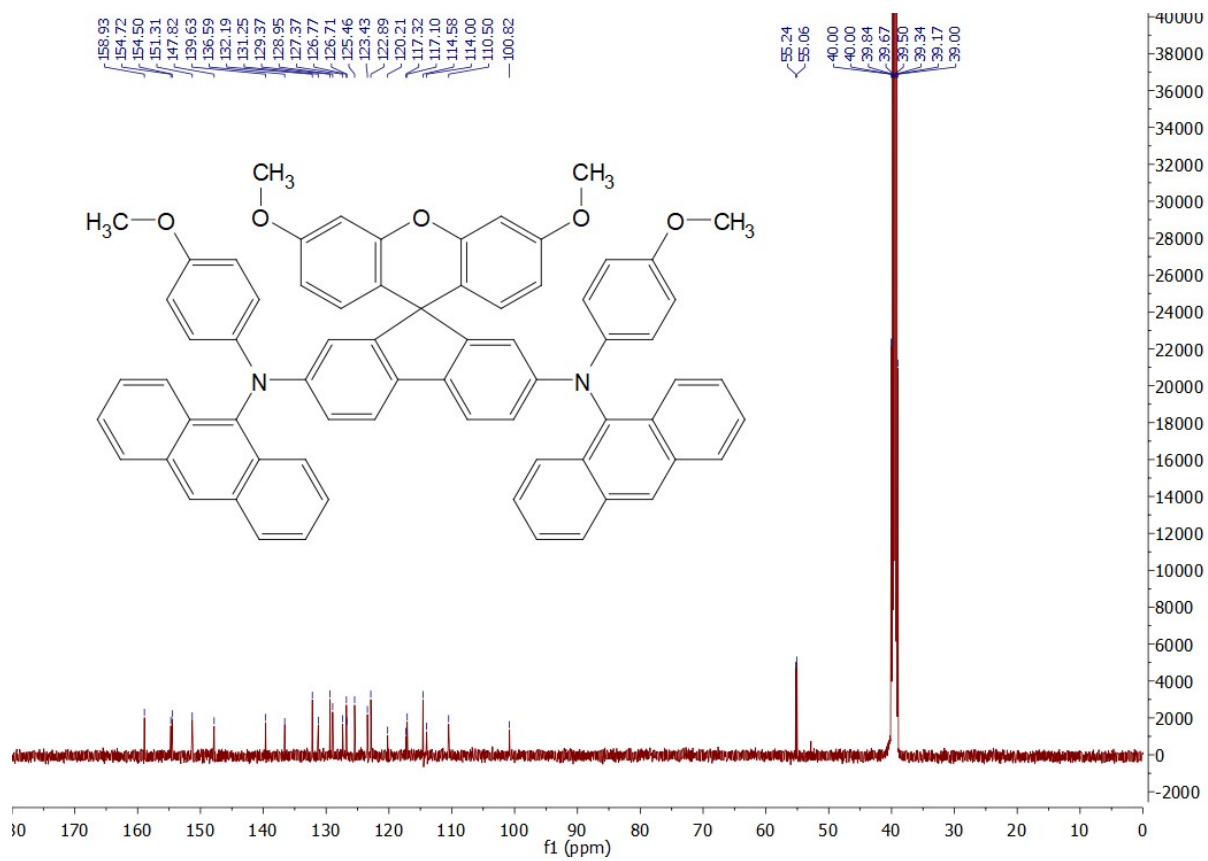


Figure S12. ^{13}C NMR (d_6 -DMSO) spectrum of X87.

SmartFormula

Formula	Mass	Error	mSigma	DblEq	N rule	Electron Configuration
$C_{69}H_{50}N_2O_5$	986.3720	0.5056	28.9034	46.00	ok	odd

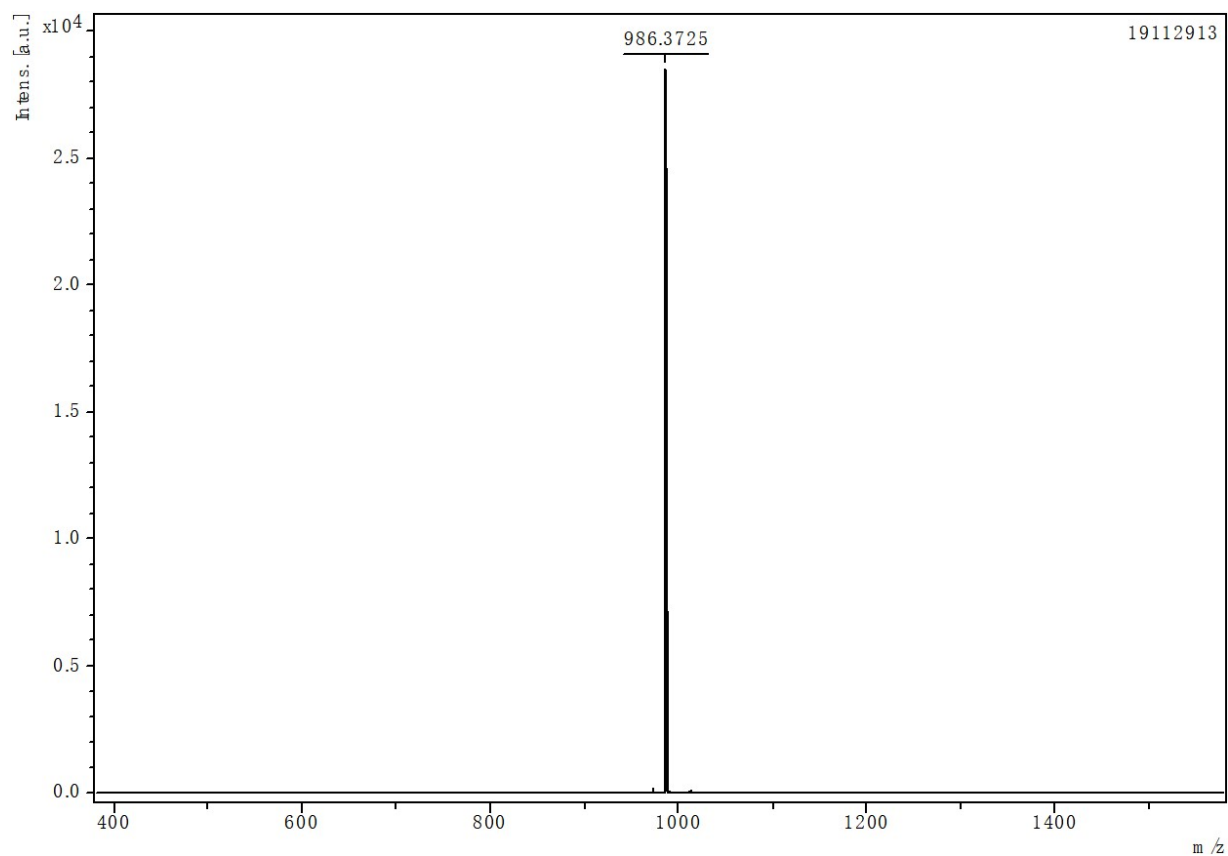


Figure S13. HR-MS spectra of **X87**.

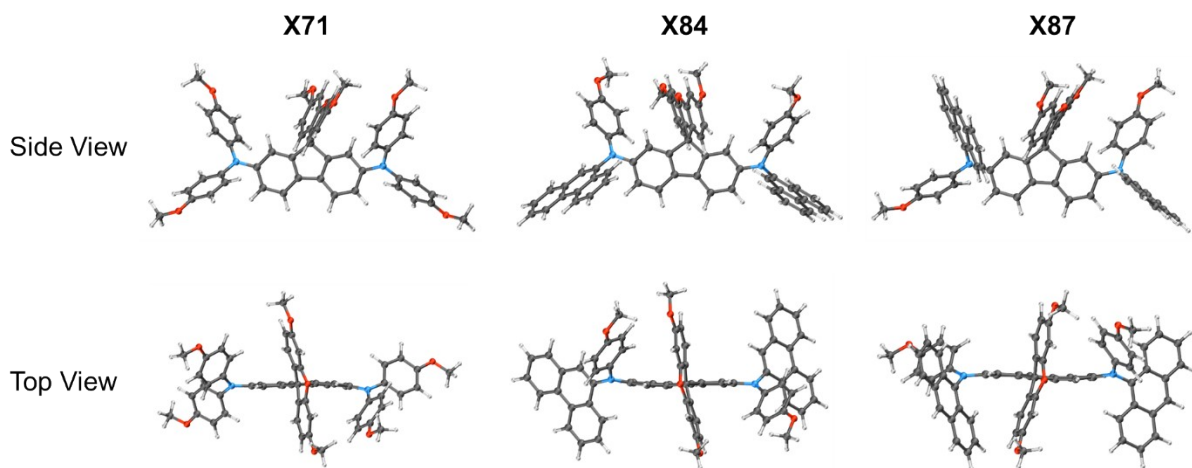


Figure S14. The optimized ground-state molecular configuration in top and side view of **X71**, **X84**, and **X87**.

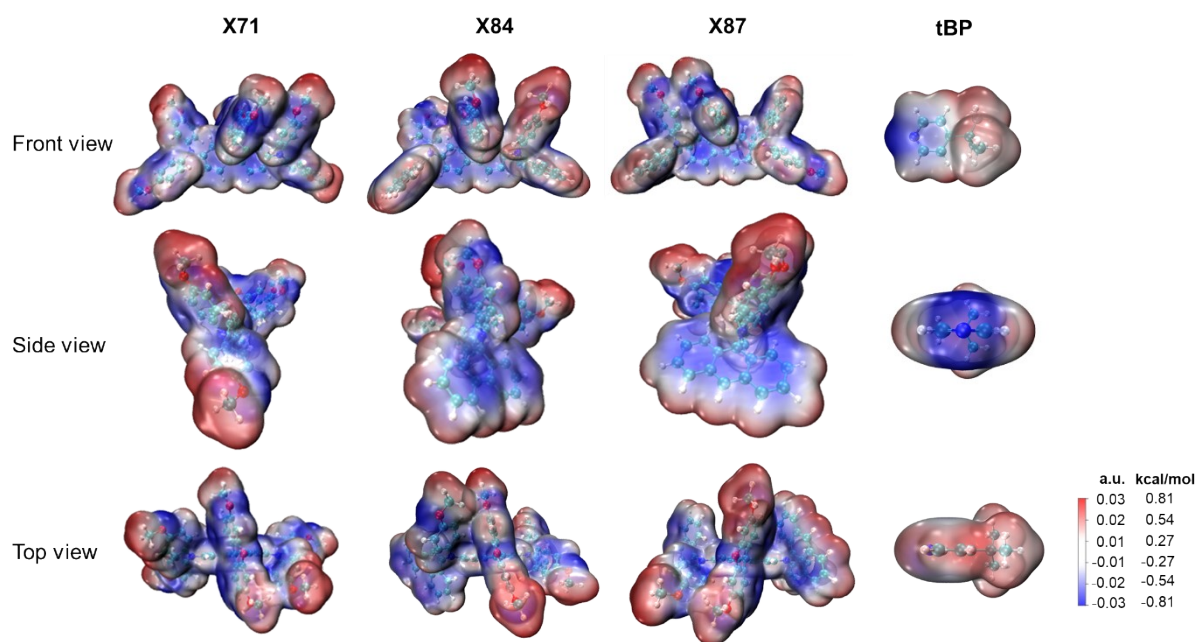


Figure S15. Electrostatic potential (ESP) surface of X71, X84, X87, and tBP.

Table S1. The crystallographic details of **X87** single crystals.

Empirical formula	C ₆₉ H ₅₀ N ₂ O ₅
Formula weight	987.11
Temperature/K	298.19
Crystal system	triclinic
Space group	P-1
a/Å	13.7579(4)
b/Å	14.1304(5)
c/Å	17.6010(6)
α/°	88.443(2)
β/°	75.156(2)
γ/°	66.642(2)
Volume/Å ³	3025.77(18)
Z	2
ρ _{calc} /cm ³	1.083
μ/mm ⁻¹	0.536
F(000)	1036.0
Radiation	CuK _α (λ = 1.54178)
2θ range for data collection/°	5.212 to 133.188
Index ranges	-16 ≤ h ≤ 16, -16 ≤ k ≤ 16, -20 ≤ l ≤ 20
Reflections collected	14138
Independent reflections	9663 [R _{int} = 0.0441, R _{sigma} = 0.0589]
Data/restraints/parameters	9663/0/690
Goodness-of-fit on F ²	1.040
Final R indexes [I ≥ 2σ (I)]	R ₁ = 0.0621, wR ₂ = 0.1679
Final R indexes [all data]	R ₁ = 0.0956, wR ₂ = 0.1881
Largest diff. peak/hole / e Å ⁻³	0.19/-0.17

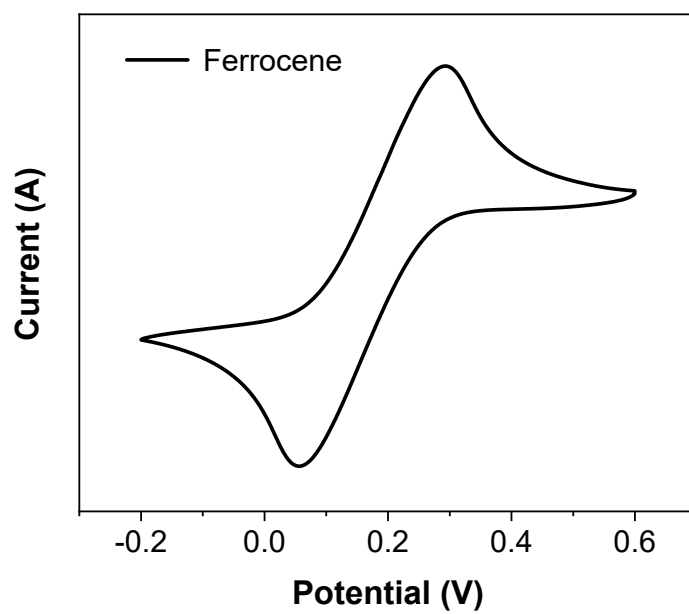


Figure S16. Cyclic voltammetry of ferrocene in the THF solution.

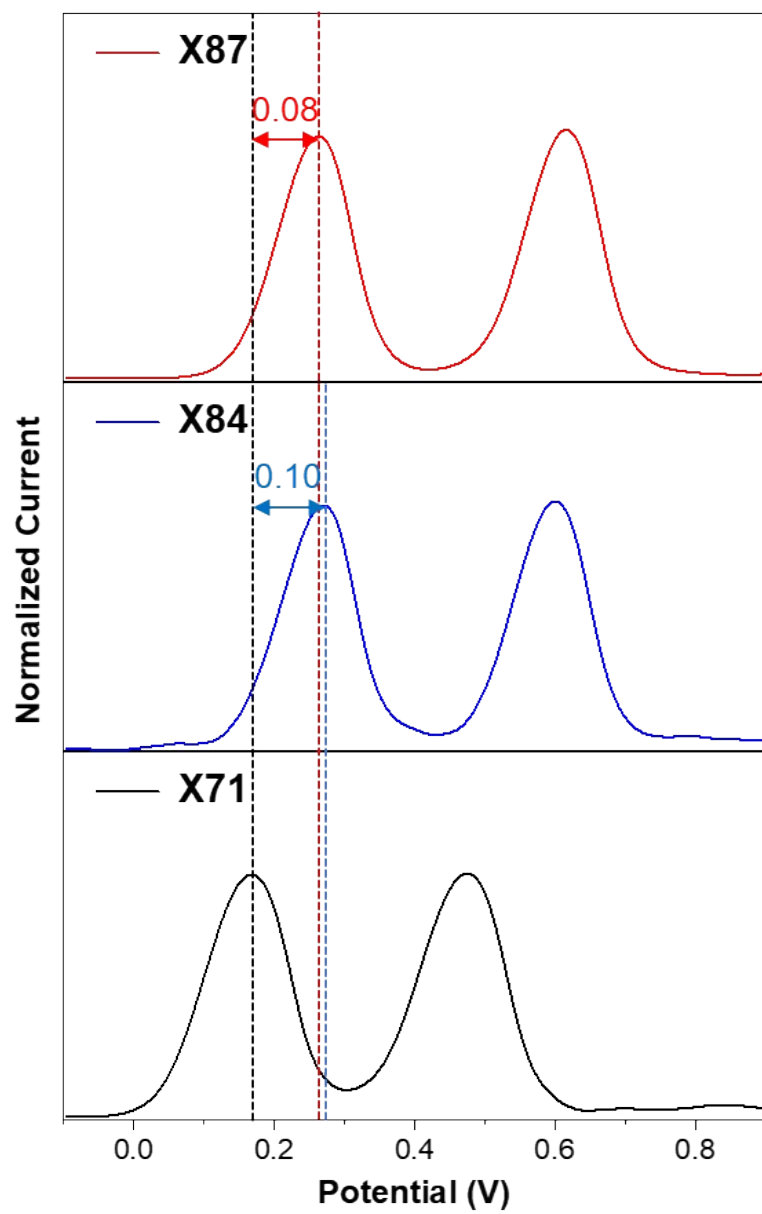


Figure S17. DPV curves of X71, X84, and X87(10^{-4} M in THF).

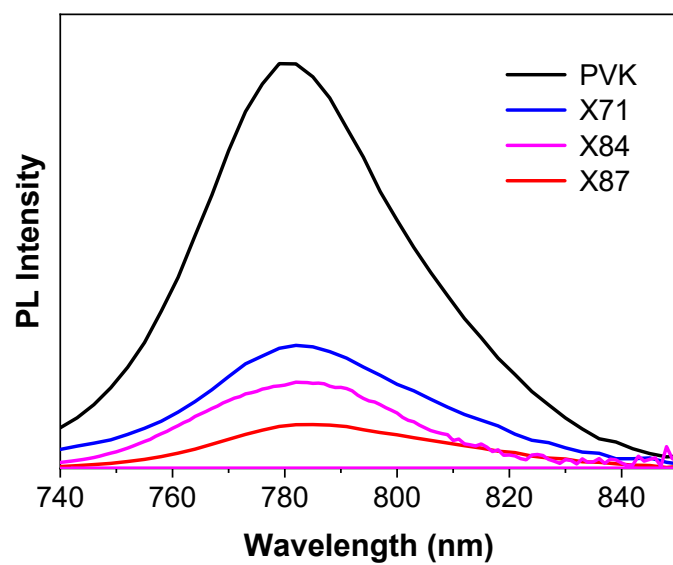


Figure S18. Steady-state PL spectra of the pristine perovskite film and HTMs coated perovskite films.

Table S2. Fitted parameters of TRPL decay curves of perovskite covering with HTMs.

Sample	τ_1 (ns)	A_1 (%)	τ_2 (ns)	A_2 (%)	τ_{ave} (ns)
X71	187.82	45.4	697.44	54.6	604.20
X84	1.05	58.7	248.71	41.3	247.23
X87	0.72	76.4	99.93	23.6	97.66

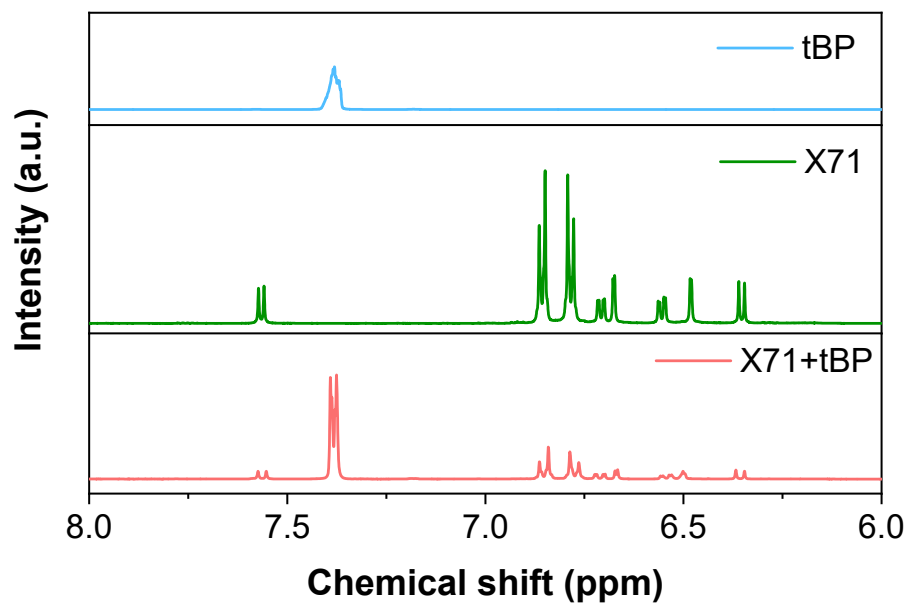


Figure S19. ¹H NMR of tBP, X71, and X71+tBP.

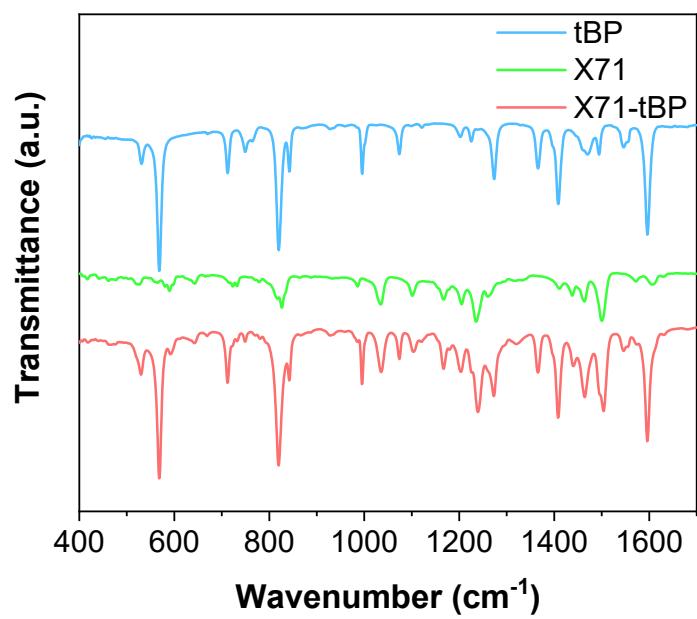


Figure S20. FTIR spectra of tBP, X71, and X71+tBP.

Table S3. Device performances based on X87 (20 devices).

Samples	J_{SC} (mA·cm ⁻²)	V_{OC} (V)	FF (%)	PCE (%)
1	24.88	1.155	80.82	23.22
2	24.51	1.155	80.19	22.71
3	24.63	1.147	80.93	22.86
4	24.10	1.149	81.58	22.60
5	24.50	1.169	79.92	22.89
6	24.35	1.154	80.02	22.49
7	24.73	1.164	81.61	23.49
8	24.55	1.154	81.77	23.16
9	24.50	1.174	79.75	22.93
10	24.35	1.152	81.08	22.74
11	24.73	1.141	82.93	23.42
12	24.74	1.139	82.81	23.34
13	24.75	1.152	82.37	23.48
14	24.22	1.135	82.9	22.80
15	24.56	1.138	81.12	22.70
16	24.33	1.166	79.77	22.63
17	24.25	1.141	79.47	22.00
18	24.88	1.181	81.95	24.07
19	24.86	1.180	81.48	23.91
20	24.68	1.175	79.21	22.97

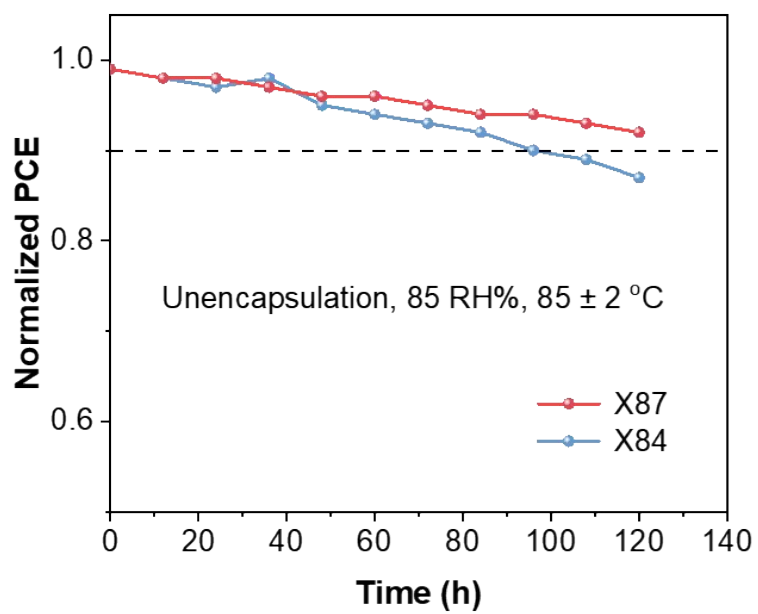


Figure S21. Normalized PCE of the unencapsulated PSCs measured in 85% RH and 85 °C in the dark.

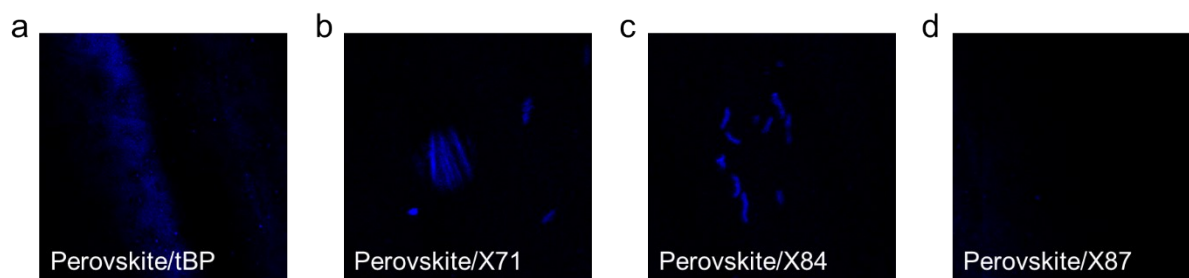


Figure S22. Fluorescence optical microscope images of the perovskite layer after aging 48 h.

The tBP and HTL were removed by chlorobenzene.

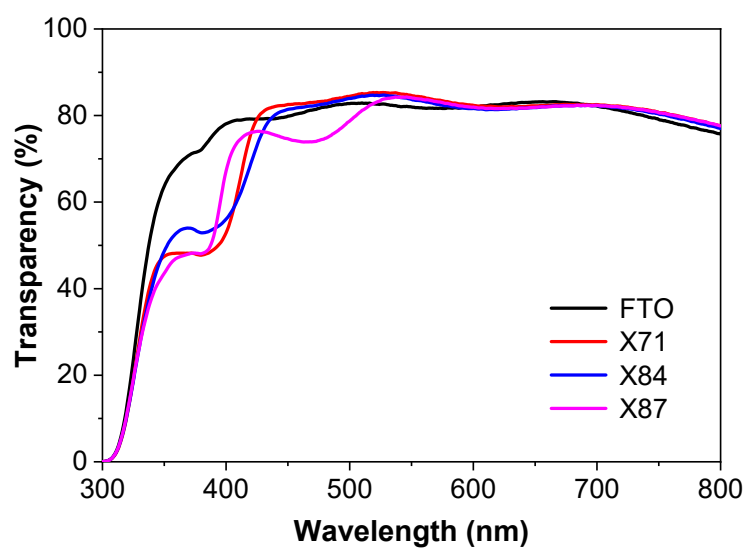


Figure S23. Transparency of FTO, X71, X84, and X87.

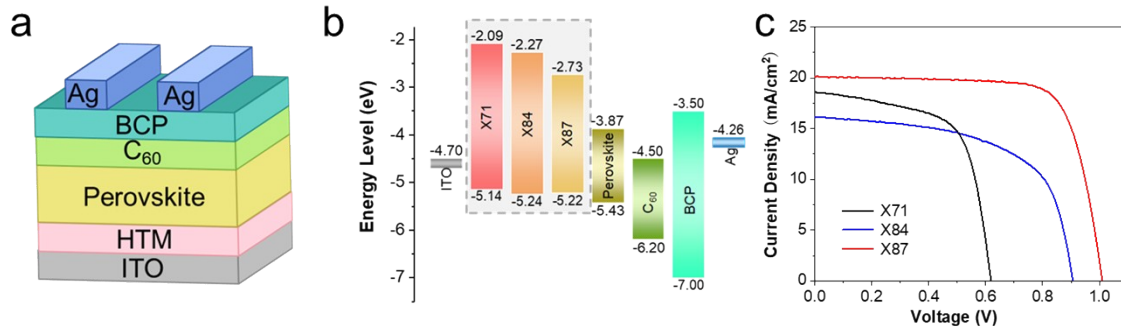


Figure S24. (a) Device structure of the p-i-n PSCs. (b) Energy level diagram of the PSCs with three HTMs. (c) J-V curves of the champion p-i-n PSCs with undoped HTMs.

Table S4. Performance parameters of optimal p-i-n PSCs with **X71**, **X84**, and **X87**.

HTMs	J_{SC} (mA·cm ⁻²)	V_{OC} (V)	FF	PCE (%)
X71	18.6	0.63	0.64	7.5
X84	16.2	0.91	0.60	8.8
X87	20.2	1.02	0.77	16.1

References

- [1] Gaussian 09, Revision E.01, M. J. Frisch, G. W. Trucks, H. B. Schlegel, G. E. Scuseria, M. A. Robb, J. R. Cheeseman, G. Scalmani, V. Barone, B. Mennucci, G. A. Petersson, H. Nakatsuji, M. Caricato, X. Li, H. P. Hratchian, A. F. Izmaylov, J. Bloino, G. Zheng, J. L. Sonnenberg, M. Hada, M. Ehara, K. Toyota, R. Fukuda, J. Hasegawa, M. Ishida, T. Nakajima, Y. Honda, O. Kitao, H. Nakai, T. Vreven, J. A. Montgomery, Jr., J. E. Peralta, F. Ogliaro, M. Bearpark, J. J. Heyd, E. Brothers, K. N. Kudin, V. N. Staroverov, T. Keith, R. Kobayashi, J. Normand, K. Raghavachari, A. Rendell, J. C. Burant, S. S. Iyengar, J. Tomasi, M. Cossi, N. Rega, J. M. Millam, M. Klene, J. E. Knox, J. B. Cross, V. Bakken, C. Adamo, J. Jaramillo, R. Gomperts, R. E. Stratmann, O. Yazyev, A. J. Austin, R. Cammi, C. Pomelli, J. W. Ochterski, R. L. Martin, K. Morokuma, V. G. Zakrzewski, G. A. Voth, P. Salvador, J. J. Dannenberg, S. Dapprich, A. D. Daniels, O. Farkas, J. B. Foresman, J. V. Ortiz, J. Cioslowski and D. J. Fox, Gaussian, Inc., Wallingford CT, 2013.
- [2] J. Zhang, B. Xu, M. B. Johansson, N. Vlachopoulos, G. Boschloo, L. Sun, E. M. Johansson and A. Hagfeldt, *ACS Nano*, 2016, **10**, 6816.
- [3] J. Zhang, Y. Hua, B. Xu, L. Yang, P. Liu, M. B. Johansson, N. Vlachopoulos, L. Kloo, G. Boschloo, E. M. J. Johansson, L. Sun and A. Hagfeldt, *Adv. Energy Mater.*, 2016, **6**, 1601062.

- [4] X. S. Li, M. Haghshenas, L. Q. Wang, J. Huang, E. Sheibani, S. C. Yuan, X. Luo, X. H. Chen, C. T. Wei, H. Y. Xiang, G. Baryshnikov, L. C. Sun, H. B. Zeng and B. Xu, *ACS Energy Lett.*, 2023, **8**, 1445-1454.
- [5] G. Xie, J. Wang, S. Yin, A. Liang, W. Wang, Z. Chen, C. Feng, J. Yu, X. Liao, Y. Fu, Q. Xue, Y. Min, X. Lu and Y. Chen, *Angew. Chem. Int. Ed.*, 2024, **63**, e202403083.
- [6] Z. Y. Xia, X. Z. Feng, T. Wu, W. Zhang, C. Chen, L. Q. Wang, W. B. Zhang, H. X. Wang, Y. Tian, Y. Hua, H. Chen and M. Cheng, *Adv. Funct. Mater.*, 2024, **34**, 2408423.
- [7] B. H. Sun, P. Z. Zhang, D. Q. Zhang, W. F. Chu, Y. X. Guo, X. Luo, W. Li and B. Xu, *ACS Materials Lett.*, 2025, **7**, 265-274.